IAC-18-B4.6B.11
Attitude and Orbit Control Results of the GOMX-4 Tandem CubeSat Mission

Rasmus Holst[1,*], Jens Nielsen[2]

GomSpace ApS, Aalborg, Denmark

David Gerhardt[3]

Orbital Wisdom LLC, Seattle, WA, USA

Jose Angel Gutierrez Ahumada[4]

Delft University of Technology (TU Delft), The Netherlands

Abstract

This paper introduces the AOCS results obtained during the first 6 months of the GOMX-4 mission, a tandem mission with two 6U CubeSats developed by GomSpace. GOMX-4A is intended for monitoring air and sea traffic in the Arctic regions while the GOMX-4B satellite is an In-Orbit Demonstration mission by the European Space Agency demonstrating several new payloads, actuators and sensors. The mission has strict requirements on inter-satellite station keeping and pointing performance due to the inter-satellite radio link between the two satellites and optical payloads on-board.

The pointing performance of the ADCS is assessed in both satellites during the early operations phase and compared to the performance obtained after a series of on-orbit calibrations of the sensors. Given satellites are designed with redundant sensors on-board (coarse- and fine sun sensors, low- and high grade gyroscopes, low- and high grade magnetometers), what makes it possible to compare the performance of the system when using different sensor configurations. Moreover a new Star Tracker, specifically tailored for the nano-satellite industry, is utilized on-board GOMX-4B as a payload. Throughout the mission of GOMX-4B, the Star Tracker will be implemented with the ADCS to eventually improve the accuracy of the pointing performance.

Another main topic of the work done with GOMX-4 relies on the Orbit control and particularly the station-keeping of the two satellites formation. CubeSats are typically launched as secondary payloads and usually do not have the capabilities to change their orbits significantly. For that reason, differences in the injection parameters of the satellites will lead to an unwanted and potentially problematic drift along-track over time.

To control the relative distance between the satellites and mitigate the initial drift, a mix of drag management and propulsion is used. The difference in the exposed surface area between the two satellites makes it possible to control the decay rate and can eventually be used for station keeping. A cold gas thruster system on-board GOMX-4B is used to perform a rapid change in the difference between the satellites orbital semi-major axis. This second part of the paper will describe how these two approaches can be combined to control the relative distance evolution with a limited amount of propellant. Throughout the GOMX-4 mission a number of propulsion maneuvers will be scheduled to reach certain reference distances and perform tests with the experimental inter-satellite radio link.

1. Introduction

Small satellite constellations have the potential to revolutionize humanity's relationship to space & earth alike. However, two key technologies require development before the power of these constellations can be fully harnessed: small satellite orbit control and inter-satellite communication. Demonstrations of these technologies form the cornerstone of the GOMX-4A/4B dual 6U CubeSat mission.

GOMX-4A is developed for the Danish Defence Acquisition and Logistics Organisation with the intention to monitor ship- and aircraft traffic in the Arctic region, especially around the Danish territory in Greenland where land-based monitoring of traffic is impractical. Previous missions such as GOMX-1 and GOMX-3 have proven the capability to monitor aircraft traffic from CubeSats, where GOMX-4A is intended to refine the infrastructure towards having low-latency surveillance from space to the end user.

*Corresponding author

Email address: rasmus@gomspace.com (Rasmus Holst)

[1] GOMX-4 ADCS Lead

[2] GomSpace ADCS Engineer

[3] Ph.D., Systems Engineer

[4] MSc in Aerospace Engineering, Student

GOMX-4B is funded by the European Space Agency (ESA) as an In-Orbit Demonstration (IOD) CubeSat, which "finds flight opportunities for innovative technologies" [1]. This program reduces risk stepwise, allowing advanced technologies to trickle up (into larger programs which have a lower risk ceiling) or across (into other demonstration missions which rely on them to test more advanced technologies). Nanosatellites are an ideal platform for these technology demonstration missions. Their small form-factor allows them to piggyback on larger missions at low cost. Additionally, as the basic functionality of nanosatellite technology matures, more missions have a stable platform on which to test advanced technologies.

The Danish company GomSpace is a leader in the development and maturation of technologies necessary for nanosatellites, and has previously demonstrated their capabilities with GOMX-1 [2] (the first CubeSat to acquire ADS-B signals in-orbit), and GOMX-3 [3] (the first ESA IOD CubeSat). Both satellites completed their mission successfully and operated in-orbit for well over their design lifetime.

2. GOMX-4A/B Satellites

2.1. Mission

The GOMX-4B mission takes advantage of the GOMX-4A project to de-risk miniaturized technologies and demonstrate system-level capabilities that will enable the controlled deployment, operation and maintenance of future operational constellation systems based on CubeSats including GOMX-4A. In particular, GOMX-4B will use an on-board propulsion module from NanoSpace to perform along-track station acquisition maneuvers relative to GOMX-4A up to separation distances representative of an operational constellation of 2000-4500 km. The relative attitudes of the two satellites will then be controlled to demonstrate differential drag station-keeping maneuvers. S-band Inter-Satellite Link (ISL) transceivers will be embarked on both GOMX-4A and GOMX-4B and operated over this range of separation distances to demonstrate low latency payload data relay to ground stations located in Danish territory. Additionally, High Speed Link capabilities shall be also tested using a similar S-band communication link between both space segments and the GomSpace Ground Station.

The achieved mission timeline is shown in Figure 1. The mission was initialized with kick off in mid-2015, completing PDR in March 2016, CDR in December 2016 and QAR in July 2017. The launch was originally scheduled to take place on a Long March 2D rocket in mid-August 2017 but was delayed until February 2nd 2018. The satellites were commissioned on April 4 2018.

2.2. System Design

The GOMX-4A/B mission spawned a lot of product development to meet the mission objectives, including

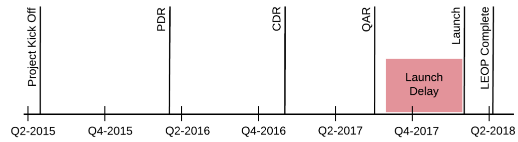

Figure 1: The GOMX-4 project time line

an all-new ADCS sensor and actuator layout. The internal components of GOMX-4B can be seen in Figure 2. Common components for both satellites include UHF- and S-band TMTC radios, S-band inter-satellite communication, GomSpace P60 EPS and a NanoMind A3200 mission OBC. The ADCS components included in both satellites are:

- **NanoMind A3200 ADCS**: An OBDH responsible for hosting the ADCS system, connecting the sensors and actuators and handling telecommands and telemetry. The A3200 board carries a low-grade magnetometer for backup purpose as well as a low-power gyroscope for coarse pointing purpose. These sensors are denoted "onboard" as they are placed on the PCB of the NanoMnind.

- **NanoSense M315 Magnetometer**: A small high-quality magnetometer capable of being placed in a magnetically quiet place inside the satellite structure.

- **NanoSense Fine Sun Sensors** are mounted on all six sides of the spacecraft. They have a field of view of 60 degree (half cone) which lets the satellite have full sun sensor coverage.

- **NanoSense Coarse Sun Sensors** are placed on all sides as in the case of the fine sun sensors.

- **Sensonor STIM210 gyroscope** included for testing purpose to increase the eclipse performance compared to what was seen on GOMX-3.

- **NovAtel OEM615 GNSS** is a dual frequency GNSS receiver using GPS and GALILEO used as input to the onboard orbit propagator. An associated antenna is placed on the +X side, facing Zenith during normal pointing attitude.

- **NanoTorque GST600 Magnetorquer** is a 3-axis magnetorquer setup consisting of magnetorquer-rods in the X- and Y directions and an aircoil in the Z direction to give a compact design.

- **NanoTorque GSW600 Reaction Wheels** are suitable for 6U missions and larger platforms developed for the GOMX-4 satellite. Four reaction wheels are mounted in a PC104-mountable pyramid configuration for redundancy purpose. The individual wheel is capable of producing a torque of up to 2 mNm with a momentum storage of 19 mNms.

GOMX-4A has an additional GNSS receiver for testing purposes:

- **NovAtel OEM719 GNSS** is a GNSS with similar specifications as the OEM615 and is included to perform flight qualification of the device as it is to replace the OEM615.

In addition to the baseline ADCS the GOMX-4B satellite includes the following extra ADCS components:

- **NanoSpace Cold Gas Propulsion Module** is a propulsion system capable of producing a thrust of 4 mN. It carried 120 grams of butane at launch, with an ISP of 59 s the module is capable of applying more than 9 m/s to the satellite.

- **ISIS Star Tracker** an experimental star tracker from Innovative Solutions In Space (ISIS) is included as a payload in GOMX-4B. After general commissioning the star tracker can be used as input to the ADCS and as verification of the ADCS performance when using the baseline sensors.

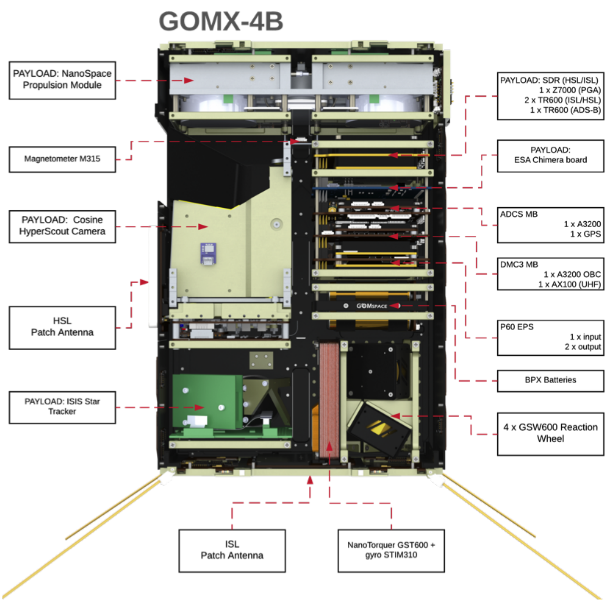

Figure 2: The GOMX-4B internal layout diagram, identifying the position of all hardware within the structure.

2.3. Payloads

The satellites include payloads necessary to complete the mission objectives such as:

- GOMX-4A **GomSpace NanoCam with 70 mm optics**

- GOMX-4A **Satlab AIS receiver**

- GOMX-4A **GomSpace ADS-B receiver**

- GOMX-4B **Cosine Hyperspectral camera**

- GOMX-4B **ISIS Star Tracker**

- GOMX-4B **ESA Chimera RHAB** (The Radiation Hardness Assurance Board) The goal of this payload is to perform In-orbit Demonstration and radiation test on SPI memories.

On both satellites a camera can be used to verify the performance of the ADCS pointing performance. Future work in the mission is to characterise the exact offset between the camera boresights and ADCS reference frame given a series of images in order to use the imagers as ADCS performance verification. Examples of images used for landmark verification from GOMX-4A and GOMX-4B is shown in Figure 3 and 4.

Figure 3: Landmark tracking from the Nanocam in GOMX-4A. Northern Jutland (DEN) in FOV.

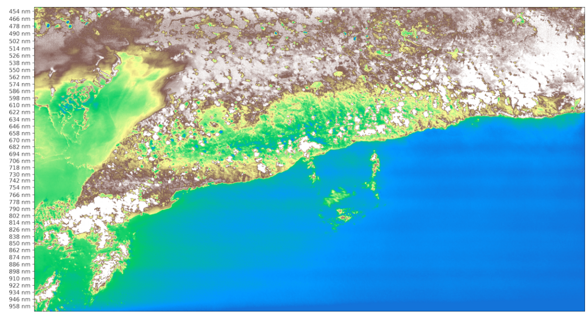

Figure 4: Hyperspectral landmark tracking from GOMX-4B. Southern Cuba in FOV. Photo: ESA / Cosine Research

2.4. *Launch*

GOMX-4 was launched on February 2nd 2018 with a Long March 2D rocket from Jiuquan, China. The satellites were inserted into a 503 km sun synchronous orbit with an LTAN of 02:11. Both satellites established two-way contact in the first day.

3. ADCSSIM Software-in-the-Loop Simulator

Many aspects of attitude determination and control systems are difficult or impossible to replicate in a lab. Often, simulation is the best method of verification available, especially for resource-constrained projects. Because of this, GomSpace has developed a dynamic simulation environment for the purposes of ADCS characterization, tuning, and verification.

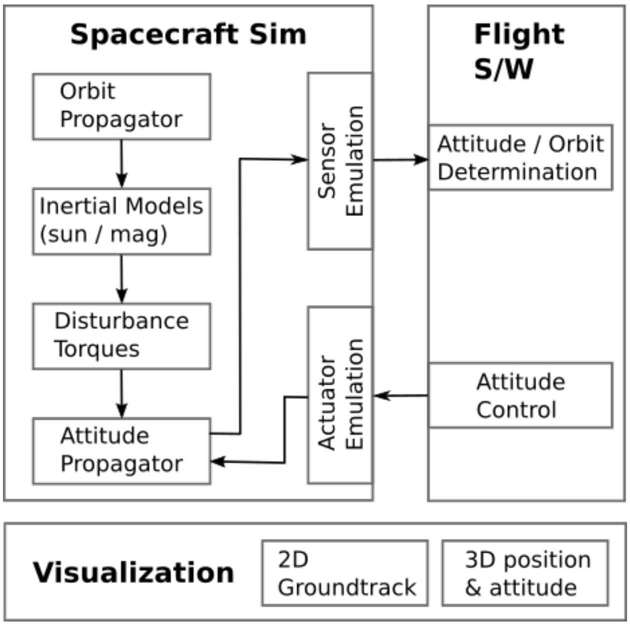

Figure 5: Components of the ADCSSIM Simulator.

3.1. *Simulation Environment*

ADCSSIM is built within the Simulink environment of Matlab. Drag & drop functional blocks allow for low complexity and ease of reuse. The main blocks of the simulation are shown in 5. The simulation is 3DOF: attitude is fully dynamic, while position is defined by a user-supplied Two-Line Element (TLE). The simulink environment allows for full Sofware-in-the-Loop simulation through the use of S-functions. In this way, the flight sofware (FSW, written in C) is compiled within Simulink for fast and accurate simulation. The spacecraft simulation emulates the sensors (FSW input) and accepts control signals (FSW output). The spacecraft simulation accounts for disturbance torques and provides a source of truth for the FSW knowledge and pointing estimation.

3.2. *Inertial Models & Sensor Emulation*

ADCSSIM uses a J2000 sun position model accurate to $< 0.01°$ over the 1950 - 2050 period [4]. The IGRF model [5] is used to calculate the local magnetic field at every position within the orbit; the accuracy of this model varies depending on space weather activity. However, NOAA estimates that minor G1-level storm conditions (Kp=5 with a planetary average of about 1 mG magnetic deflection [6]) occur less than 25% of the days in a full 11-year solar cycle [7]. This deviation roughly matches the post-calibration error of the magnetometer (see Section 4.1).

Each sensor discussed in Section 2.2 has its own model based on characterization data. Error characterization such as offset/bias, scale, Gaussian noise, quantization, misalignment, and temperature-based scale/offset are employed.

3.3. *External Torques & Attitude Dynamics*

Disturbance models for solar radiation pressure, atmospheric drag, gravity gradient, and residual magnetic torques are calculated. Control torques are emulated using actuator models for the reaction wheels and magnetorquers. The sum of the disturbance torques and control torques are fed into Euler's rotational equation of motion as external torques. This equation is numerically integrated using the variable-step ode45 solver, along with the quaternion kinematic differential equation to propagate the attitude.

3.4. *Validation*

The first defense against simulation error is a visualization block within ADCSSIM; it features both 2D groundtrack and 3D orbit and attitude capabilities. Second, ADCSSIM builds on flight experience and development for many missions: Ørsted, AAUSAT I & II, SSETI Express, GOMX-1, and GOMX-3. Finally, ADCSSIM output has been validated against similar models developed at ESA.

4. Sensor Calibration & Characterization

4.1. *Magnetometer*

Magnetometers are subject to errors from nearby hard- and soft-magnetic sources. On the ground, calibration normally occurs by collecting raw data while rotating each sensor through the majority of the attitude sphere, and fitting calibration constants against a known constant B-field magnitude [8]. GOMX-4 improved upon the ground-based calibration with an on-orbit magnetometer calibration [9] which compares against a truth estimated from the IGRF magnetic field model [5]. As shown in Figure 6, the on-orbit calibration restores the error mean to near-zero while significantly decreasing the magnetometer noise. These plots use measurements collected from the NanoSense M315 magnetometer.

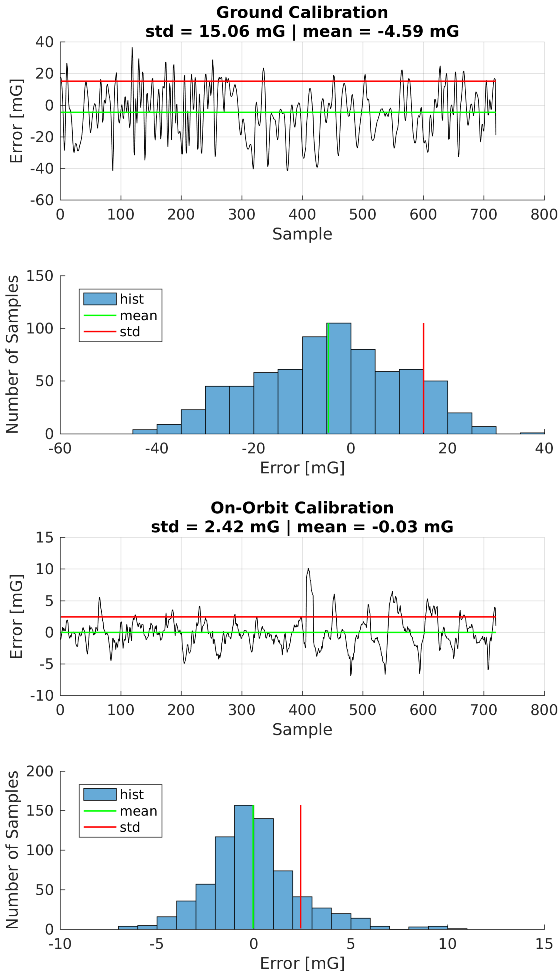

Figure 6: GOMX-4B Magnetometer Calibration: ground-based (top) vs. on-orbit calibration (bottom). The same 20 hr dataset is shown in both plots. The attitude-independent error magnitude is calculated by comparing the post-calibration output to the IGRF magnetic field model.

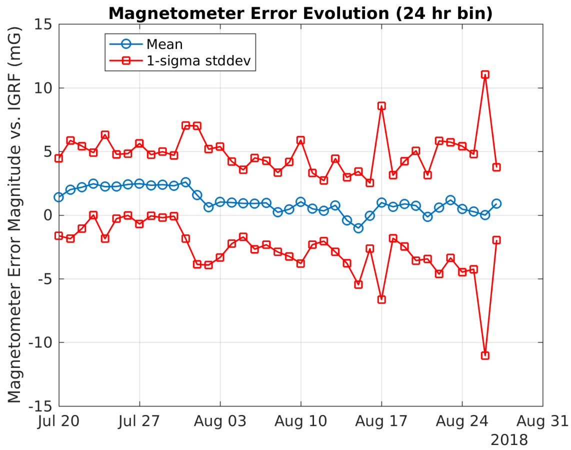

Figure 7: GOMX-4B Magnetometer Calibration Drift: the evolution of magnetometer error over time is shown for a single a free-float calibration performed using data collected on 2018.07.20.

The Unscented Kalman Filter requires an estimate of the magnetometer measurement noise. Because of this, the time-dependence of the magnetometer noise was investigated; see Figure 7. The magnetometer error (vs. IGRF) was binned into 24-hour periods and plotted over a 35 day duration. Some variation in the true local magnetic field is expected due to space weather impacts. As shown, over the entire period, the error mean / standard deviation is approximately 1 mG / 4 mG, respectively.

4.2. Rate Gyro

GOMX-4B contains two rate gyros, identified by their relationship to the A3200 ADCS computer: either 'onboard' or 'external'. The former is an industrial-grade gyro while the latter is an experimental tactical-grade gyro. In order to characterize the performance of the gyros, an Allan Variance test was performed by collecting over 6 hours of data at a 35 Hz frequency. Figure 8 shows the Allan Deviation from the measurement and compared to the ADCSSIM sensor model; the plot uses the Output Angle method for calculating the Allan Deviation [10]. When compared to the external gyro, the onboard gyro Angle Random Walk (Allan deviation at a 1 sec time cluster size) is approximately 2× larger and the Bias Instability (zero-slope Allan deviation) is approximately 10× larger. The ADCSSIM external gyro model is a good match for the external gyro measurement data, while the ADCSSIM onboard gyro model diverges from measurement at larger cluster sizes (although the bias instability is roughly matched).

A simulation-based sensitivity study was carried out to investigate the impact of the rate gyro on the satellite ADCS performance. ADCSSIM was used to simulate the ADCS performance difference between the two available gyros. In both cases, the simulation was tuned to the rate gyro by matching the UKF knowledge uncertainty to the knowledge error; this ensures good performance from the gyro. As an attitude sensor, the rate gyro has the largest impact on the knowledge error, which is shown in Figure 9. The figure shows that while insolation performance is much the same, there is significant divergence between the gyro performance in eclipse, where only a single observation vector (magnetic field) is available. All subsequently-shown ADCSSIM output and on-orbit measurements use the external gyro.

4.3. GNSS Receiver

The GNSS receiver outputs a Cartesian state vector of ECEF position and velocity, along with an epoch time. Characterization needs a model to compare individual measurements. Because of the ubiquity of the Two-Line Element (TLE), an orbit determination method to convert individual GNSS state vectors to a TLE was developed. The quasi-constant mean orbit elements which compose the TLE (such as the semi-major axis) can then be compared. It is important to note that characterization of the GNSS receiver deals with error introduced

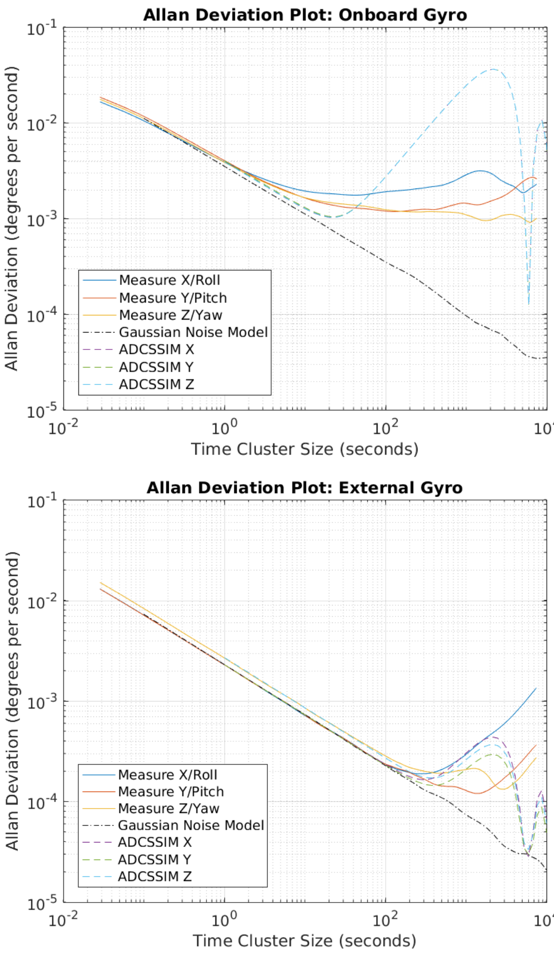

Figure 8: Allan Deviation for the two rate gyros aboard GOMX-4B: onboard gyro (top) vs. external gyro (bottom). The ADCSSIM sensor model is shown along with the measurement.

by the orbit determination method used, as well as noise from the sensor itself.

The variance of the mean element estimation sets the baseline for the ability to observe changes in the orbit of a satellite. To investigate this, GOMX-4B was used to collect GNSS data over a more than 2 weeks without using its thrusters. Figure 10 shows that the GNSS-based mean orbit elements have a standard deviation of about 69 meters, after a linear fit is removed to account for drag effects.

Of course, TLEs are useful because propagation methods (i.e. SGP4) allow prediction of where the spacecraft will be in the future. In order to investigate the accuracy of this prediction, each GNSS-based TLE was propagated forward 24 hours and compared with the NORAD TLE with the closest epoch. However, the NORAD TLEs are only released at a cadence of 1 to 4 per day, so there is some scatter in the true propagation time. Figure 11 shows that 1.0±0.2 days of propagation results in a position difference (GNSS vs. NORAD) standard deviation of 6.8 km (1σ).

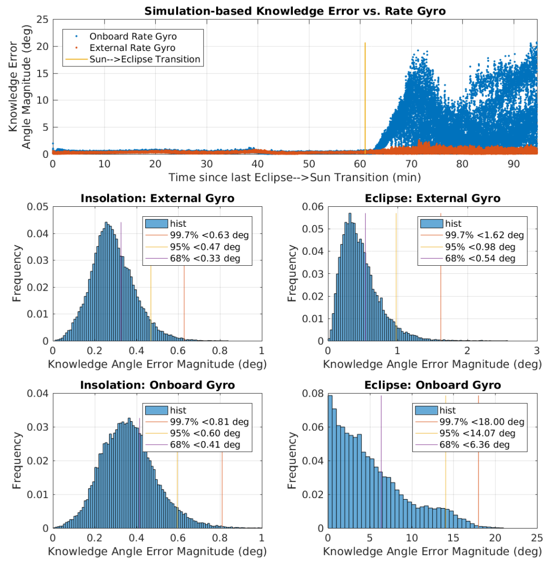

Figure 9: Simulation-based true knowledge error vs. orbit time for a 10-orbit dataset. Performance of the external and onboard rate gyros are shown, and differentiated in the histograms below, which also show the impact of insolation vs. eclipse.

4.4. *Sun Sensors*

The 6 coarse sun sensors, one on each of the sides of the satellite, are used with standard calibration as these sensors are not used with great confidence in the estimation. They are mainly used for telemetry purpose. The 6 fine sun sensors, also located on each side of the satellite, are calibrated on ground prior to being mounted on the satellite body. This leaves a small but unknown offset between the sensor and satellite body due to mounting tolerance. An on-orbit calibration to calculate the offset using the ephemeris data and magnetometer is applied. This method compares the calculated angle between the sun vector and the B-field vector with the angle between the measured B-field (assuming a well calibrated magnetometer) and the sun sensor. None of the sun sensor types are using an active Albedo correction. The results of the in-orbit calibration of the sun sensors are seen in Table 4.4. The error includes the sun sensor error as well as the magnetometer error as per calibration description.

Fine Sun Sensor Performance	**Error**
Ground Calibration	6.84 deg
On-orbit Calibration	1.50 deg
On-orbit Calibration, 60 deg FOV limited	1.16 deg

Table 1: Sun sensor error when comparing sun sensor measurement with magnetometer measurement.

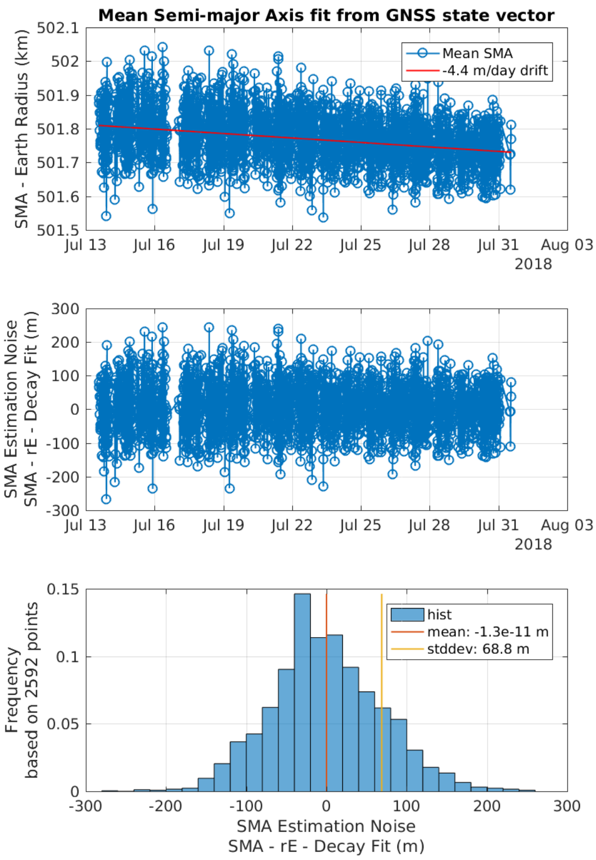

Figure 10: The GNSS receiver was used to estimate the GOMX-4B mean semi-major axis. After a -4.4 m/day linear fit was removed to account for drag effects, an estimation noise of 69 m (1σ) was found.

5. Filter Tuning

GOMX-4B relies on an Unscented Kalman Filter (UKF) for attitude determination. This Bayesian filter use a priori estimates of process and measurement noise to form the best possible state estimate using noisy measurement data. Thanks to its statistical nature, it also estimates the covariance (i.e. uncertainty) of the state estimate at each timestep. However, all Kalman filters require some level of tuning and/or characterization to establish trust in the filter's estimates of state and uncertainty. Both simulation- and on-orbit telemetry-based tuning are used here.

The on-orbit data used in this section was collected by commanding GOMX-4B to stay fixed to an LVLH-frame for a period of 10 orbits, starting 2018.08.29 at 18:21 UTC. In this pointing mode, +X (3U face) is aligned to zenith, +Y (6U face) is aligned with orbit normal, and +Z (2U face) is roughly facing Ram (though not exactly due to the non-circular orbit of the GOMX-4 spacecraft).

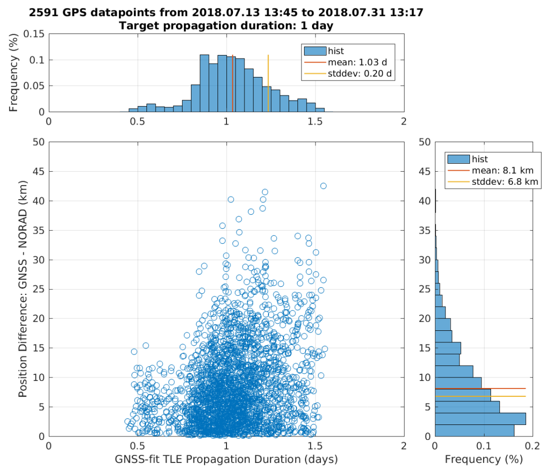

Figure 11: GNSS-based TLEs were propagated roughly 24 hours, to the epoch of the closest-available NORAD TLE. The SGP4-based Cartesian position difference magnitudes are then calculated.

5.1. *Simulation-based Tuning*

Simulation-based tuning seeks to align the simulated filter's estimated state covariance with the simulated true error. For example, a properly-tuned 1-sigma knowledge uncertainty estimate should bound approximately 68% of the true knowledge error. As stated above, the ADCS engineer has two levers with which to tune the filter: the measurement noise covariance (the expected level of noise inherent to each attitude sensor) and the process noise covariance (the expected amount of noise in state propagation). As one could expect, the measurement noise covariance has fields for the coarse sun sensors, the fine sun sensors, and the magnetometer. Good values for measurement noise covariance can be derived from sensor characterization (see Section 4).

The process noise covariance accounts for unknown or unmodeled sources of noise (i.e. position-based inertial model errors, space weather impacts to drag / B-field modeling, etc.) by accounting for a fixed amount of Gaussian noise. When compared with measurement noise covariance, it is often more difficult to assign appropriate values to process noise covariance, but this variability makes the process noise covariance an excellent lever for tuning. The UKF aboard GOMX-4B uses two states: the error quaternion (3-element vector part only), and the rate gyro bias. For simplicity, the UKF is also built with the same two sources of process noise. To a certain extent, the rate gyro characterization has a direct feedthrough to the rate gyro process noise, but in general, both elements of process noise are varied manually until the distributions for UKF-estimated state covariance and simulated true error are well-aligned. Figure 12 shows the post-tuning comparison of ADCSSIM-based estimated attitude knowledge uncertainty and error. Tuning is often best-effort: although many of the distributions are quite similar, none of them match exactly. Although the estimated uncertainty generally overestimates the true error, in the sun it is within 0.5° of the truth, and in eclipse it is within 1° from the truth. Currently, the UKF implementation uses the same covariance value for all axes of a given measurement / process. Future work could improve performance by allowing axis-specific covariance values.

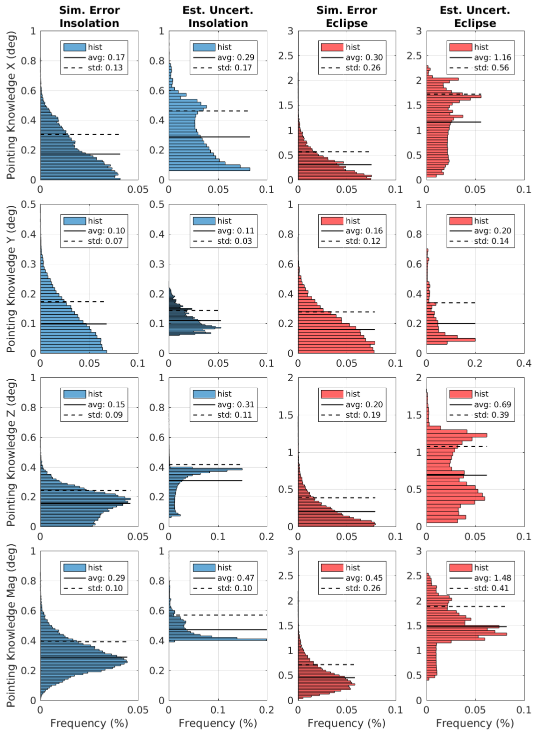

Figure 12: Histograms of simulated attitude knowledge uncertainty vs. error for each axis (plus overall magnitude), separated into insolation and eclipse performance. For ease of comparison, the axes have the same scale for each insolation state / axis combination.

5.2. *On-Orbit Telemetry-based Tuning*

With the simulation-based tuning parameters in hand, the next step is to implement the tuned filter on-orbit, and analyze the data received from the on-orbit asset. There are two ways to check for filter accuracy. First, using only the on-orbit data, we can compare the innovation (difference between measured vs. UKF-modeled attitude observation) with the UKF's innovation covariance. These values are already calculated during the UKF filtering process, so there is minimal extra onboard processing to access these data. Figure 13 shows such a comparison for the magnetometer aboard GOMX-4B; the filter is well-tuned for this sensor, as the innovation covariance mean is close to the innovation standard deviation for axes X & Z. The plot also shows that the UKF currently overestimates the uncertainty of the Y-axis. This could be corrected with an axis-specific covariance setting, or it could be attributed to the specific reference attitude used during the time of data collection (described above).

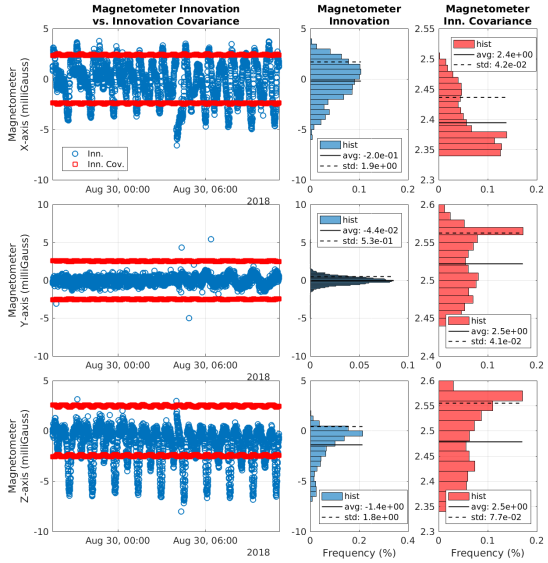

Figure 13: The magnetometer's innovation and innovation covariance calculated by GOMX-4B over a 10 orbit period while referenced to the LVLH frame.

The second telemetry-based tuning method is less straightforward. Because the true error is not observable in reality, we can compare the on-orbit UKF knowledge uncertainty estimate with the simulated UKF knowledge uncertainty estimate. We can then build confidence in the simulation's estimate of the UKF performance (and thus the simulation-based tuning) by observing how well the on-orbit UKF matches the simulated UKF. Figure 14 shows this comparison for the 10-orbit dataset. As shown, the measurement and simulation are very well matched in terms of UKF output. This is also apparent in Figure 15 which is discussed below. This gives good confidence in ADCSSIM and provides a basis for trusting the simulation-based error estimates given above.

6. Attitude Performance

Missions are often defined by a single, high-level descriptor of their pointing ability: the Absolute Pointing (APE) Error, the true difference between where the satellite is actually pointed and where it is desired to point. Ideally, an independent absolute attitude sensor with significantly higher accuracy (i.e. star tracker or imager) would be used during tuning to provide a source of truth to compare with the onboard UKF estimate of pointing error (the 'perceived' pointing error) and the onboard UKF estimate of the knowledge error. However, such independent data sources are often not easy to obtain: they require slew maneuvers and/or large data transfer times. Ground-based simulation is another

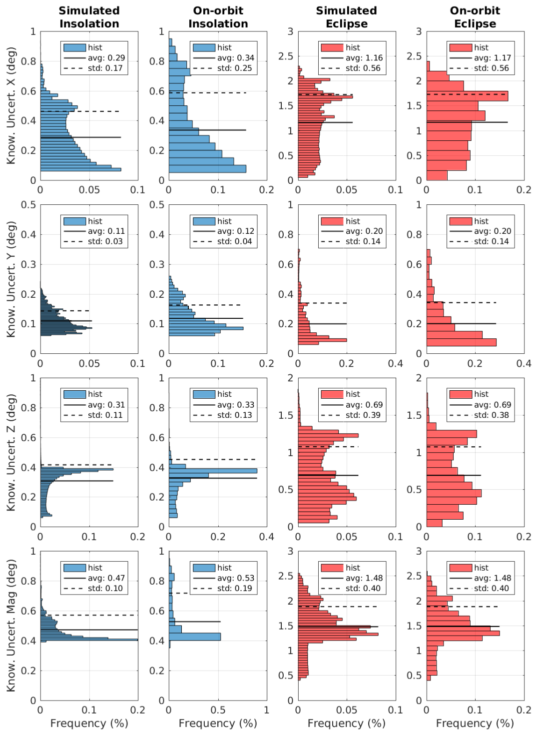

Figure 14: Histograms of estimated knowledge uncertainty as calculated by GOMX-4B vs. ADCSSIM for each axis (plus overall magnitude), separated into insolation and eclipse performance. For ease of comparison, the axes have the same scale for each insolation state / axis combination.

source of APE, although it comes with a caveat: the simulation must be closely matched to reality.

In order to estimate how well-aligned ADCSSIM is with reality, a 10-orbit LVLH-aligned dataset was captured from GOMX-4B. The same time and control modes were simulated using ADCSSIM and the two datasets were compared. First, the performance of the attitude knowledge estimation is compared in Figure 15. As shown, the on-orbit- and simulation-based UKF estimates of knowledge uncertainty are very well matched. Second, both estimates contain the majority of the simulated knowledge error. This suggests the true knowledge error is well-bounded by the 1-sigma knowledge uncertainty estimates.

Figure 16 shows a comparison of the measurement-based estimate of pointing error (and uncertainty) vs. the pointing error estimated by ADCSSIM. Here we see a significant difference between the on-orbit data and ADCSSIM for insolation periods; this difference is attributed to ADCSSIM not accounting for albedo, a key error source for fine/coarse sun sensors. Interestingly, the perceived pointing error actually decreases in eclipse periods when such sensors are not available. Future work will investigate reducing the use of sun sensors and/or including an albedo model within ADCSSIM.

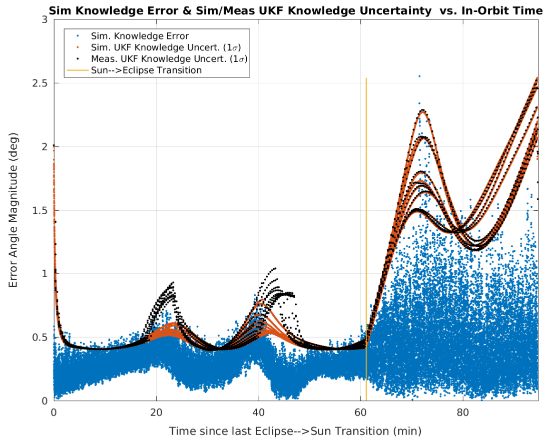

Figure 15: Knowledge error estimates from the on-orbit UKF (black dots) and ground-based simulated UKF output (red). These are compared with a simulation-based source of true 3-axis knowledge error, the difference between the UKF attitude estimate and the true attitude, which is shown in blue. Ten orbits of data are shown on the same plot by converting the absolute time to the relative time since the last eclipse-to-sun transition. Finally, the yellow line divides the insolation periods (left) from eclipse periods (right).

7. Orbit Control

The demand for utilizing nanosatellite for constellations and formation flying are becoming more frequent. Developing an orbit control system for Cubesats would open up the possibility to handle mission concepts where formation flying is key for performing coordinated ground coverage, an inter-satellite network, distributed sensing or extending/retracting orbital lifetime. In any case, the requirements for such a control system, would state that the satellites should be able to reach their desired relative positions within a given timeframe. For other CubeSat constellations, like Planet's Doves, the orbit control systems have been relying on passive actuation using differential drag maneuvers for commisioning and station-keeping [11]. Such maneuvers would potentially take months to perform before the satellites are optimally distributed throughout the orbit. Moreover, differential drag maneuvers also require a sufficiently large satellite surface area and a high ratio between the maximum and minimum surface area.

For the GOMX4 mission, orbit control has been demonstrated by the use of a combination between differential drag control and propulsion. The GOMX-4A and -4B satellites are flying in a tandem formation, where the relative distance between them is required to be controlled in order to perform in-orbit demonstration and verification of inter-satellite radio link. GOMX-4A is maneuvered by using differential drag and the GOMX-4B satellite is equipped with the NanoSpace 6U cold gas propulsion module. The relative distance between the two satellites are controlled by a series of

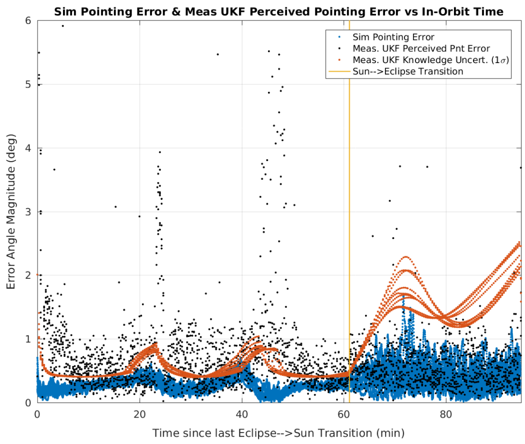

Figure 16: The on-orbit UKF estimates the pointing error (black dots) the associated pointing knowledge uncertainty (red dots). These are compared with a simulation-based estimate of the knowledge error (blue dots), the difference between the simulated UKF attitude estimate and the simulated true attitude. Ten orbits of data are shown on the same plot by converting the absolute time to the relative time since the last eclipse-to-sun transition. The yellow line divides the insolation periods (left) from eclipse periods (right). The plot has an upper limit of 6 degrees for clarity; this does not show 19 of the measured UKF perceived pointing error data (approximately 0.7% of the full dataset), which reach a maximum of 11.2 degrees.

prograde and retrograde thrusting maneuvers, adjusting the orbit semi-major axis and thereby also the orbit velocity of GOMX-4B. After the final thrusting maneuver, station-keeping maneuvers are performed by the use of differential drag maneuvers between the satellites. By varying the relative satellites surface area, the decay rate can be adjusted and varying the satellites semi-major axis and thereby the change in relative distance. Hereby, station-keeping can be made without the use of cold gas thrusters, to mitigate for relative drift caused by control errors and mass differences between the satellites.

7.1. GOMX4 Orbit Maneuvers

As stated before, drag management using different drag surfaces in both satellites and the propulsion module on-board GOMX-4B conform the two main ways to control the orbital evolution of the satellites and in particular the distance between them. As expected before launch, the satellites were injected by the launcher into two slightly different orbits with a difference in semi-major axis of approximately 300 meters, mainly due to the fact that there was a span of 30 seconds between the deployment of both satellites. This difference, which was quickly confirmed after launch, may seem small but leads to a difference in orbital period that produces a relatively quick drift between the satellites.

During the first few weeks after launch (February 2nd 2018), the altitude difference led to a drift of approximately 50 km/day. Once full-on attitude control was established, GOMX-4A and GOMX-4B followed a high-drag and low-drag attitude mode, respectively, in order to decrease the altitude of 4A relative to 4B and slow down the drift. This process proved to be slow, decreasing the drift rate to approximately 40 km/day as of March 14th 2018. The inter-satellite distance was already around 2,000 km at this point and the Inter-Satellite Link (ISL) required a shorter distance for running initial tests, hence it was decided to use the thrusters on-board GOMX-4B to raise its orbit and revert the sense of the drift.

Figure 17 and 18 shows the evolution of the inter-satellite distance and the altitude of both satellites, respectively, since launch until now. Five stages, clearly delimited by four propulsion maneuvers, can readily be distinguished:

- From launch until the first propulsion maneuver (March 14th 2018), the satellites have an altitude difference of more than 300 meters and they drift by approximately 50 km/day, as stated before. GOMX-4B was lower than GOMX4-A and therefore leads the formation.

- The prograde maneuver on March 14th 2018 raises the altitude of GOMX-4B by 600 meters, what reverts the drift and starts bringing the satellites closer. A retrograde maneuver on April 17th 2018 decreases the altitude of GOMX-4B to approximately 50 meters higher than that of GOMX-4A. The drift is slowed down significantly, with GOMX-4A slowly approaching GOMX-4B until they overlap around May 7th 2018.

- At this point, a prograde maneuver raises again the orbit of GOMX-4B to allow for a faster and controlled separation, in this case with GOMX-4B trailing GOMX-4A in the formation. From this point on the satellites were undergoing a performance testing of the ISL. This approximately constant separation rate is maintained until a 2,250 km separation on June 29th 2018.

- A final retrograde maneuver on this date matches the altitude of both satellites to stop the drift. From this point, the separation rate is controlled using exclusively drag management, with the separation varying slowly between 2,250 km and 2,500 km.

The breakdown of the mission presented above shows the capabilities of propulsion and drag management for controlling the altitude and separation of nanosatellites in long-range formation flying. Propulsion becomes necessary when the altitude difference is significant, since the effect of high-drag and low-drag attitude is not sufficient to produce a large altitude change in a reasonable amount of time.

7.2. Orbit Simulation Tool

The propulsion maneuvers were planned using simulations run with NASA's General Mission Analysis Tool (GMAT) [13]. The simulation employed orbital parameters retrieved from TLE's provided by NORAD [12],

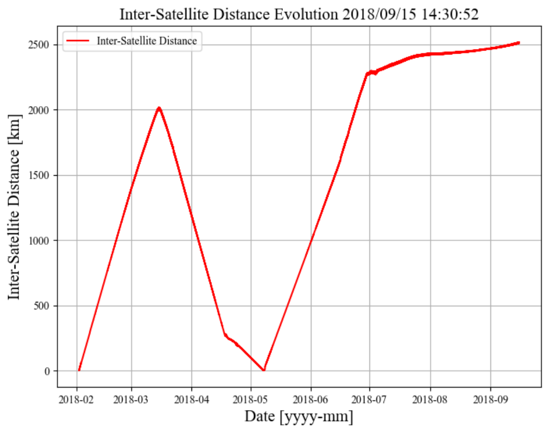

Figure 17: Evolution of the inter-satellite distance since launch, processed from historical TLE data provided by NORAD [12].

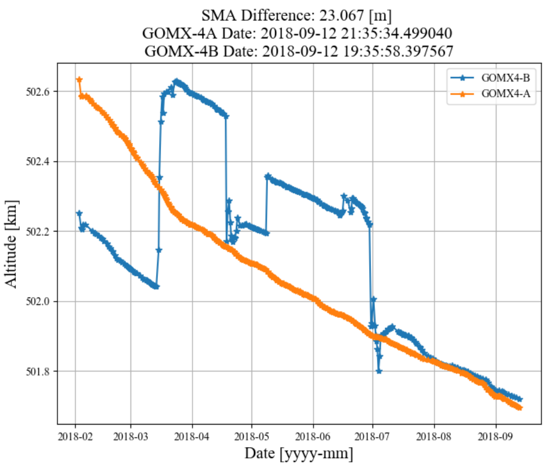

Figure 18: Evolution of the altitude of GOMX-4A and GOMX-4B since launch, processed from historical TLE data provided by NORAD [12].

along with the physical specifications of the satellites, the propulsion module on-board GOMX-4B and a high-fidelity model implemented with the following dynamics:

- Non-spherical gravity of the Earth (up to degree and order 36).
- Point-mass gravity of the Sun and the Moon.
- Spherical (cannonball) solar radiation pressure.
- MSISE90 atmospheric model (with F10.7 = 150 and Magnetic Index = 3).

A differential corrector solver determines the duration of the burns necessary to achieve a certain semi-major axis, as well as the length of the coasting phase between propulsion maneuvers that leads to the desired separation between the satellites.

Because it was initially determined that very long burns could pose a strain to the AOCS system (with potential wheel saturation) as shown in Figure 19, each propulsion maneuver was divided into several burns of a few minutes along consecutive orbits that can be monitored from ground. The total propellant consumption of each maneuver was also predicted using GMAT and proved to be very accurate when compared with the actual amount of propellant consumed.

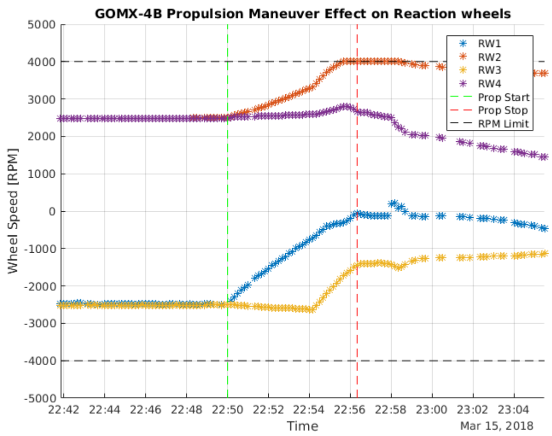

Figure 19: The resulting external torques, compensated by the reaction wheels, caused by Centre of Mass (CoM) misallignment versus propulsion thrust vector.

8. Conclusion

8.1. Lessons Learned

A number of lessons learned have occurred during the development phase and operations phase of the mission. Some of the lessons learned from previous GOMX missions can be found in [14]. The appended lessons are itemized below:

- **Representative model is invaluable**: This was already discovered during the earlier missions but cannot be highlighted enough. The ability of testing and planning scenarios on an satellite Engineering Model (EM) ensures to utilize the available satellite pass time. With two different Flight Models (FM) satellites in the mission, carrying different payloads, it has been possible to configure the EM to represent the individual FM with only minor configurations needed to change identity of the EM between representing GOMX-4A or GOMX-4B. This work was done in the design phase of the mission when configuring the hardware options, EPS power channels and network addresses to the satellites in a way that makes them as identical as possible.
- **Automated telemetry check is useful**: The time needed to monitor the daily ADCS telemetry in

the two GOMX-4 satellites, along with other satellites, is growing as more features and components are introduced. In order to lower the task of looking through telemetry a system has been developed to monitor the telemetry for any outliers outside a predefined interval for the parameters of interest. This has proven to save a lot of time during daily operations of the satellites.

- **Automatic satellite operations utilizes link time**: During the operations phase, the autopilot software used in the earlier missions have been improved in a way, where it is now able to command the satellite with tasks. This is especially helpful for the passes over the Aalborg ground station outside normal work hours, as the satellites are loaded with tasks and data payload data is collected also during night and weekends without operators in the loop.

8.2. Next Steps

- **Verification**: For the remaining part of the mission it is planned to get the pointing verified by use of a imager. The ideal scenario would be to use the ISIS star tracker to output a quaternion and compare that to the estimated attitude from the ADCS. Alternatively one of the imagers can be used to verify the pointing by detecting landmarks on the images, although this alternative would take more processing.

- **Star Tracker implementation**: When the payload commissioning of the star tracker onboard GOMX-4B is done, it would be ideal to use the attitude estimate of the star tracker as a sensor in the ADCS. Most of the interface for this is already in place, the main work lies in retuning the UKF to take in the star tracker measurement in the same way as described in Section 5 for the other sensors.

9. Acknowledgements

A big thank you to goes to the GNC team at ESTEC, ESA for the help during the design phase of the mission and help to supply models for the sloshing analysis.

Another thank you should be given to the GOMX4 team and the remaining personnel at GomSpace for the cooperation throughout the mission.

[1] About in-orbit demonstrations, `http://www.esa.int/Our_Activities/Space_Engineering_Technology/About_In-orbit_demonstrations`, accessed: 2016-04-20.

[2] L. K. Alminde, K. Kaas, M. Bisgaard, J. Christiansen, D. Gerhardt, GOMX-1 Flight Experience and Air Traffic Monitoring Results, in: Small Sat Conference, 2014, pp. 1–7.

[3] D. Gerhardt, M. Bisgaard, L. Alminde, R. Walker, M. Fernandez, A. Latiri, J.-L. Issler, GOMX-3: Mission Results from the Inaugural ESA In-Orbit Demonstration CubeSat, in: Small Satellite Conference, 2016.

[4] D. A. Vallado, Fundamentals of Astrodynamics and Applications, 3rd Edition, Microcosm Press, 2007.

[5] C. C. Finlay, S. Maus, C. D. Beggan, T. N. Bondar, A. Chambodut, T. A. Chernova, A. Chulliat, V. P. Golovkov, B. Hamilton, M. Hamoudi, R. Holme, G. Hulot, W. Kuang, B. Langlais, V. Lesur, F. J. Lowes, H. Lühr, S. Macmillan, M. Mandea, S. McLean, C. Manoj, M. Menvielle, I. Michaelis, N. Olsen, J. Rauberg, M. Rother, T. J. Sabaka, a. Tangborn, L. Tø ffner Clausen, E. Thébault, A. W. P. Thomson, I. Wardinski, Z. Wei, T. I. Zvereva, International Geomagnetic Reference Field: the eleventh generation, Geophysical Journal International 183 (3) (2010) 1216–1230. doi:10.1111/j.1365-246X.2010.04804.x.
URL `http://doi.wiley.com/10.1111/j.1365-246X.2010.04804.x`

[6] The k-index, `https://www.swpc.noaa.gov/sites/default/files/images/u2/TheK-index.pdf`, accessed: 2018-08-13.

[7] Noaa space weather scales, `https://www.swpc.noaa.gov/sites/default/files/images/NOAAscales.pdf`, accessed: 2018-08-13.

[8] C. Foster, G. Elkaim, Extension of a two-step calibration methodology to include nonorthogonal sensor axes, Aerospace and Electronic Systems 44 (3).
URL `http://ieeexplore.ieee.org/xpls/abs\_all.jsp?arnumber=4655364`

[9] J. C. Springmann, J. W. Cutler, Attitude-Independent Magnetometer Calibration with Time-Varying Bias, Journal of Guidance, Control, and Dynamics 35 (4) (2012) 1080–1088. doi:10.2514/1.56726.

[10] Allan variance: Noise analysis for gyroscopes, Tech. Rep. AN5087, Freescale Semiconductor (February 2015).
URL `http://cache.freescale.com/files/sensors/doc/app_note/AN5087.pdf`

[11] C. Foster, H. Hallam, J. Mason, Orbit Determination and Differential-Drag Control of Planet Labs Cubesat Constellations, AIAA Astrodynamics Specialist Conference.
URL `https://arxiv.org/pdf/1509.03270.pdf`

[12] Norad, `https://www.celestrak.com/NORAD/elements/cubesat.txt`, accessed: 2018-09-13.

[13] Gmat, `https://software.nasa.gov/software/GSC-17177-1`, accessed: 2018-03-01.

[14] I. A. Portillo, D. Gerhardt, M. Bisgaard, Launch and Early Operations Phase for the GOMX-3 Mission, in: 2nd Latin American CubeSat Workshop, 2016, pp. 1–13.